Improved Algorithm for On-line Harmonic Identification in HVDC Application

H.R. Najafi
University of Birjand, IRAN
h.r.najafi@birjand.ac.ir

F. Robinson
University of Bath, UK
F.V.P.Robinson@bath.ac.uk

A. Shoulaei
Iran University of Science & Technology,
shoulaei@iust.ac.ir

***Abstract*- The application of a newly developed algorithm is presented which allows the on-line measurement and tracking of the time-varying harmonic content of distorted voltage and current waveforms arising at the point of connection between HVAC and HVDC power systems. A novel discrete Kalman filtering technique is used which is able to rapidly acquire and accurately track the values of harmonic amplitudes and phases. The effectiveness of the presented method is demonstrated by a simple test case. Amplitude and phase acquisition is compared with that of an on-line FFT-based frequency scanner. The proposed algorithm has been applied in the identification and tracking of the harmonic content of waveforms obtained at the point of HVAC/HVDC common coupling. However, the technique is suitable for more general power system and power electronic applications where the rapid and accurate acquisition of harmonic properties is required.**

I. INTRODUCTION

One of the most important problems when HVAC and HVDC systems are connected is the interaction between these systems. Of major concern are the disturbances arising from the generation of harmonics which often lead to serious operating problems in practical HVDC systems. This issue has attracted significant attention in HVDC literature for reasons now briefly considered.

The switched, non-linear behavior of HVDC phase-controlled thyristor converters causes the injection of the harmonic currents into the connected AC system. This generates characteristic harmonics under steady-state conditions and non-characteristic harmonic during transient changes [1]. The harmonic components produce undesirable effects both within the HVDC and HVAC systems, such as greater instability and loss of precision in the control and protection systems, greater heat production and power loss in components and conductors, and they generate greater noise and interference within local control and telecommunication systems. For the reduction of undesirable effects, the accurate identification of voltage and current harmonic content is very important. Having insight into the levels of harmonics and waveform distortion aids the design of appropriate filters for good steady-state operation, and the optimal adjustment of controller and compensation equipment parameters under transient conditions [1,2].

With a steady HVDC-converter firing-angle, fixed commutation duration, and undistorted AC system voltage conditions, an AC/DC converter produces so-called characteristic harmonics, which are a multiple of the fundamental frequency. However such idealized operation does not persist in practice and more complex current and voltage waveform spectra result. Harmonic voltages and unbalance exist on the AC side, and current ripple will exist on the DC side. Also, with constant–current control, the firing angle will not be steady and commutation period duration will also vary. Therefore, not only are harmonic voltages and currents transferred though the converter but also their effects may be amplified through the variation of thyristor switching instants [1]. A fast, accurate method is required to carry out the identification process and accurately track time variations in current and voltage harmonic amplitude and phase.

II. HARMONIC ANALYSIS ALGORITHMS

Most frequency-domain harmonic-analysis algorithms are based either on the Discrete Fourier Transform (DFT) or on the Fast Fourier Transform (FFT), and approximate the voltage and current frequency spectra from discrete time samples. The DFT and FFT algorithms have been usefully applied in power system phasor measurements and harmonic analysis [3,4]. However, misapplication of the FFT algorithm leads to inaccurate results [2,5]. The basic assumptions employed in the application of the DFT and FFT are that: (i) the signal is stationary (constant magnitude), (ii) the sampling frequency is equal to the number of samples multiplied by the fundamental frequency assumed by the algorithm, (iii) the sampling frequency is greater than twice the highest frequency in the signal to be analyzed, and (iv) each frequency in the signal is an integer multiple of the fundamental frequency. When these assumptions are satisfied, the results of the DFT or FFT are accurate. However, accuracy suffers when these assumptions are not true because of three effects; aliasing, spectral leakage, and picket-fence effect [5]. Aliasing can be alleviated by increasing the sampling frequency. Data acquisition system sampling rate is usually set at a fixed value, of several kHz or more. If the sampled waveform does not contain an integer number of samples per integer number of cycles, the results of the DFT algorithm will include errors. The resulting error is known as spectral leakage [2,5]. The DFT and FFT of such a sampled waveform will incorrectly indicate non-zero values for all of the harmonic frequencies. Reference [6] reviews the problems associated with direct application of FFT to compute harmonic levels of non steady-state, distorted waveforms and presents various ways to describe recorded data in statistical

terms. Recently DFT and FFT methods have been improved. For example, [7] proposes the optimization of spectrum analysis to reduce the restrictions on FFT input and consequently the picket-fence and leakage effects are reduced. Reference [8] implements a least square (LES) parameter estimation algorithm for the identification and measurement of power system harmonics. Reference [9] presents a dynamic filter based on the least absolute value algorithm for on line tracking of power system harmonics. Reference [10] presents a comparative study for power system harmonic estimation. It compares the results obtained using DFT, the LES algorithm, and the least absolute value (LAV) parameter estimation algorithm. It concluded that the three algorithms produce the same estimate, if the signal under study is free of noise. However, if some data samples are missed, the least absolute value produces a better estimate than the DFT and LSE algorithms.

The proposed harmonic amplitude and phase identification algorithm gives further improvement over the previously discussed methods and is based on Kalman filtering. Reference [11] reviews the applications of linear Kalman filter algorithms for electric power quality analysis and discusses the potential improvement possible. These applications include the measurement of harmonics and voltage sags. In this paper, a Kalman filter algorithm has been developed for the identification of harmonics associated with HVDC systems, and the output of this is directly compared with an FFT method to quantify its superior steady-state and tracking accuracy.

III. Optimal On-Line Identification

Different state-variable models have already been derived for phasor representation. They can be divided into two different categories: (a) models with a variable measurement matrix and constant transition matrix, and (b) models with variable transition matrix and constant measurement matrix. Modeling based on (b) involves greater calculation and consequently takes longer to solve, because the variable transition matrix is a full matrix. In this study, the modelling uses a variable measurement matrix, and is now considered.

The AC voltage or current input is assumed to comprise N harmonics and may be expressed as:

$$s(t)=\sum_{n=1}^{N}\left[S_{nr}(t)\cos(n\omega t)-S_{ni}(t)\sin(n\omega t)\right] \quad (1)$$

The discrete system to be estimated is described at the k^{th} time sample by the state equation:

$$x(t_{k+1})=x(t_k)+w(t_k) \qquad t_k=kT_{sf},\ k\in\aleph^{+} \quad (2)$$

In (2), T_{sf} is the sampling period, $f=\omega/2\pi$ is fundamental frequency, and $x(t_k)$ is the $2N$ dimension state-variable vector of real and imaginary components of the fundamental and harmonic phasors where:

$$x(t_k)=\left[S_{1r}(t_k)\quad S_{1i}(t_k),\ldots S_{Nr}(t_k)\quad S_{Ni}(t_k)\right]^T \quad (3)$$

Also in (2), $w(t_k)\in\Re^{2N}$ is the random variable vector that allows for time variation of the state variables. It is described, noting its zero mean and no time correlation, by its covariance matrix as:

$$Q_{w,k}=E\left[w(t_k)w^T(t_k)\right] \quad (4)$$

The measurement equation is given by:

$$z(t_k)=H_k^T x(t_k)+\upsilon(t_k) \quad (5)$$

In (5), $z(t_k)$ is the k^{th} sampled measurement of $s(t)$, and H_k is the following $2N$ vector:

$$H_k=\left[\cos(\omega t_k),-\sin(\omega t_k),\ldots,\cos(N\omega t_k),-\sin(N\omega t_k)\right]^T \quad (6)$$

Also in (5), $\upsilon(t_k)$ is the measurement noise, which is assumed to be a white sequence with known $Q_{\upsilon k}$ covariance and to be uncorrelated with the $w(t_k)$ sequence.

The Kalman filter state estimation $\hat{x}(t_k)$ at the k^{th} step is based on the recursive equation:

$$\hat{x}(t_k)=\hat{x}(t_{k-1})+K_k\left(z(t_k)-H_k^T\hat{x}(t_{k-1})\right) \quad (7)$$

where K_k, the Kalman gain, is obtained from the following recursive equation:

$$K_k=\left(\frac{1}{H_k^T\tilde{R}_kH_k+Q_{v,k}}\right)\tilde{R}_kH_k \quad (8)$$

In (8), $\tilde{R}_k$ is the prediction error covariance matrix which is obtained from:

$$\tilde{R}=E\left[\left(x(t_k)-\hat{x}(t_{k-1})\right)\left(x(t_k)-\hat{x}(t_{k-1})\right)^T\right]=\hat{R}_{k-1}+Q_{w,k-1} \quad (9)$$

In (9), $\hat{R}_k$ is the estimation error covariance matrix at the k^{th} step and is evaluated using the following recursive equation in which I is identity matrix:

$$\hat{R}_k=F_k\tilde{R}_k=\left(I-k_kH_k^T\right)\tilde{R}_k \quad (10)$$

The value and changing rate of the $\hat{R}_k$ matrix depends on its initial value, $\hat{R}_0$. The matrix $\hat{R}_k$ has a stable asymptotic behavior if the system is observable [12]. Since it is apparent that all the states are not asymptotically stable, then to assure that the sequence of $\hat{R}_k$ is upper-bounded it must be proved that all the states are observable [12,13]. To show the observability, reference must be made to the behavior of the Kalman filter every $2N$ steps.

The discrete system (2) and (3) is equivalent to the following system with $2N$-times smaller sampling frequency:

$$x(t_{(k+1),2N})=x(t_{k,2N})+\eta(t_{k,2N}) \quad (11)$$

$$\xi(t_{k,2N})=C_{k,2N}x(t_{k,2N})+v(t_{k,2N}) \quad (12)$$

where: $\eta(t_{k,2N})=\sum_{i=0}^{2N-1}w(t_{k,2N+i})$, $C_{k,2N}=\left[H_{(k-1),2N+1},\ldots,H_{k,2N}\right]^T$ $\xi(t_{k,2N})=\left[z(t_{(k-1),2N+1}),\ldots,z(t_{k,2N})\right]^T$, and $v(t_{k,2N})=\left[\left(v(t_{(k-1),2N+1})-H_{(k-1),2N+1}^T\sum_{i=1}^{2N-1}w(t_{k,2N-i})\right),\ldots,v(t_{k,2N})\right]^T$

All the states of the discrete system (11) and (12) are observable if and only if $C_{k,2N}^TC_{k,2N}$ is full rank; that is, the rows of $C_{k,2N}$ are independent vectors in $\Re^{2N}$ (observability condition). In the following it is assumed that the observability condition is satisfied, and the sequence $Q_{w,k}$ and $Q_{v,k}$ are constant matrixes q_w and q_v, respectively. From (8) and (10) it can be easily proved that matrices $\tilde{R}_k$ and $\hat{R}_k$

asymptotically reach constant values in any frame of orthogonal coordinates that jointly rotates with H_k.

The asymptotic matrices $\tilde{R}_{k,\infty}$ and $\hat{R}_{k,\infty}$ can be obtained, from the solution of (13) the steady–state Riccati Equation (SSRE), and (14), respectively. In (13), A is the rotation matrix such that $Hk_{+1} = AH_k$.

$$\tilde{R}_{k,\infty} = A^T\left(\tilde{R}_{k,\infty} - \frac{\tilde{R}_{k,\infty}H_k H_k^T \tilde{R}_{k,\infty}}{H_k^T \tilde{R}_{k,\infty} H_k + q_v}\right)A + q_w \qquad (13)$$

$$\hat{R}_{k,\infty} = \tilde{R}_{k,\infty} - \tilde{R}_{k,\infty}H_k\left(H_k^T \tilde{R}_{k,\infty} H_k + q_v\right)^{-1} H_k^T \tilde{R}_{k,\infty} \qquad (14)$$

For analyzing the asymptotic performance of the Kalman filter state estimation when starting from the initial estimate $\hat{x}_0$, the discrete system (2) and (3) with a constant expected value $E[x(t_k)] = x^\circ$ is first estimated using (15).

$$E\left[x^\circ - \hat{x}(t_k)\right] = F_k E\left[x^\circ - \hat{x}(t_{k-1})\right] \qquad (15)$$

Then the expected value of the estimation error at the k^{th} step can be derived from (7) and (10). It is apparent that F_k causes a reduction along the observable direction H_k, because:

$$H_k^T F_k H_k = \frac{q_v}{\left(H_k^T \tilde{R}_{k,\infty} H_k + q_v\right)} < 1 \qquad (16)$$

If the observability condition is satisfied so that all the directions are observable, then the sequence of expected values of estimation errors cannot diverge. Moreover, F_k being asymptotically constant in a frame of coordinates that jointly rotates with H_k, the sequence (15) must asymptotically tend to a constant value in such a form. That is, it must be given by:

$$\hat{e}_{k,\infty} = A\hat{e}_{k-1,\infty} \qquad (17)$$

where $\hat{e}_{k,\infty}$ and $\hat{e}_{k-1,\infty}$ are the asymptotic values of $E\left[x^\circ - \hat{x}(t_k)\right]$ and $E\left[x^\circ - \hat{x}(t_{k-1})\right]$, respectively. By combining (15) and (17), the following steady-state equation is obtained:

$$F_{k,\infty}\hat{e}_{k-1,\infty} = A\hat{e}_{k-1,\infty} \qquad (18)$$

where $F_{k,\infty}$ is the asymptotic value of F_k.

Starting from the definition of F_k (10), and from the solution $\tilde{R}_{k,\infty}$ of SSRE, (13), it may be shown that any non-zero solution of (18) is invalid. That is, the expected value of the estimates asymptotically tends to be unbiased.

The correlation between subsequent estimation errors can be obtained from (7) and (10):

$$\hat{R}_{k+n,k} = E\left[\left(x^\circ - \hat{x}(t_{k+n})\right)\left(x^\circ - \hat{x}(t_k)\right)^T\right] = \left(\prod_{i=1}^{n} F_{k+i}\right)\hat{R}_k \qquad (19)$$

and asymptotically:

$$\hat{R}_{k+n,k} = \left(\prod_{i=1}^{n} F_{k+i,\infty}\right)\hat{R}_{k,\infty} \qquad (20)$$

Since each term $F_{k+i,\infty}$ of the product in (20) causes a reduction along the observable direction H_{k+i}, then the sequence of matrices $\prod_{i=1}^{n} F_{k+i,\infty}$ tends to zero as $n \to \infty$. Consequently, the smallest data window, nT_{sf}, can be defined in such a way that the correlation between two different estimates of the Kalman filter is negligible.

IV. Validation and Application

A. Validation

The accuracy of the proposed optimal on-line identification algorithm was investigated by applying a test signal. The test signal has known harmonic content and its general form is given by the following equation.

$$f_{Test}(t) = \sum_h F_{Test,h}\cos(h\omega t + \varphi_{Test,h}) \qquad (21)$$

where: $\omega = 2\pi f$, and f is the fundamental frequency of the test signal. Fig. 1 shows comparison of the test signal, $f_{Test}(t)$ and its identified signal, $\hat{f}(t)$.

The agreement between them is good and the output of the algorithm faithfully tracks the test signal after a short settling interval that is shown in Fig.1a. The ongoing estimation of the magnitudes of several harmonics of the test signal in Fig. 1 (i.e. 1, 5, 7 and 11) is shown in Fig. 2. The short time taken for the algorithm to acquire an accurate estimate (about 5 ms for Fig.1) is evident.

Also, within the PSCAD/EMTDC software package [14], a test signal is derived and applied to the available On-line Frequency Scanner (OFS) FFT algorithm. Figure 3 gives superimposed fundamental harmonic magnitude and phase estimates provided by the Kalman filter and OFS FFT algorithms over time. The figures show that with similar sampling (10 kHz) the time taken by the Kalman filter algorithm to reach an accurate estimate of both magnitude and phase (T_{SKM}, T_{SKP}) is consistently smaller than that of the FFT (T_{SFM}, T_{SFP}). The steady-state accuracy of the Kalman filter algorithm is also consistently better.

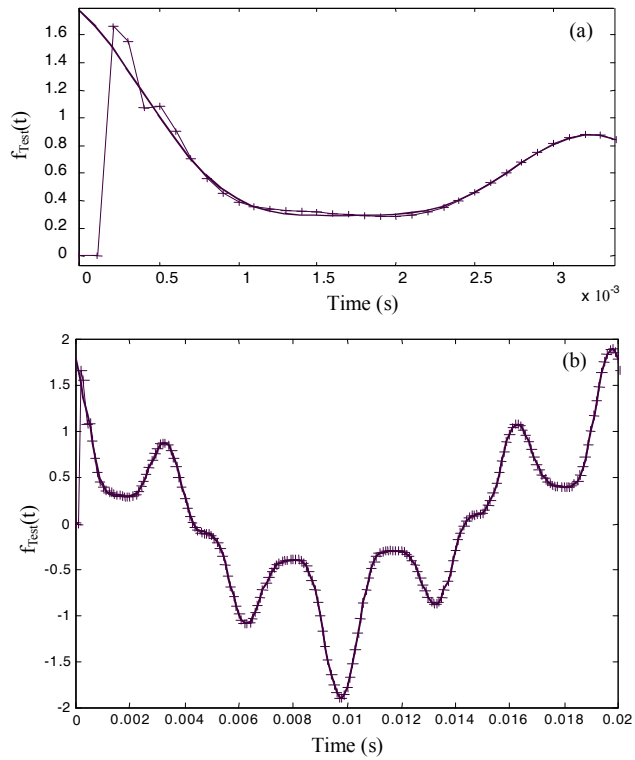

Fig. 1. Source test signal (bold line) and estimated values (feint line, +) at (a) the beginning of sampling and (b) over a line-frequency period.

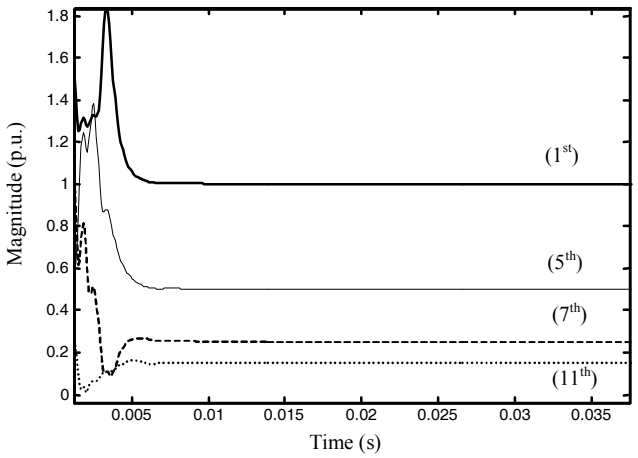

Fig. 2. Harmonic magnitudes of the Fig.1 test signal, estimated using the proposed algorithm.

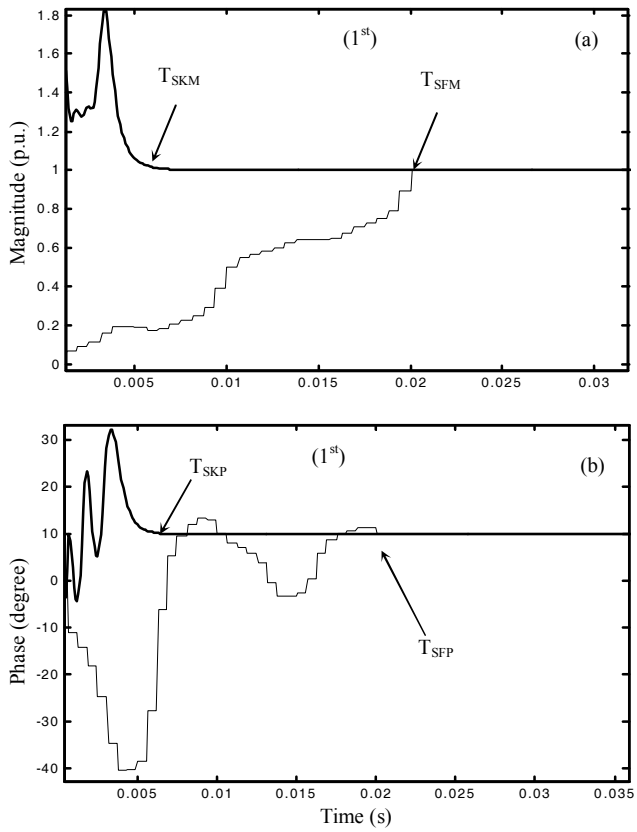

Fig. 3. Harmonic (a) magnitudes and (b) phases of the Fig.1 test signal, estimated using the OFS FFT (feint), and proposed algorithms (bold).

This is evident from the graphs of magnitude error against time shown in Fig.4. A residual error remains in the OFS FFT algorithm output; whereas the Kalman filter algorithm output settles within 1% of the actual value in half the time of the FFT algorithm and gives an exact value after 20 ms.

The faster settling and better steady-state accuracy are critically important when attempting very precise regulation or fault discrimination, especially during the dynamic operation of a power system.

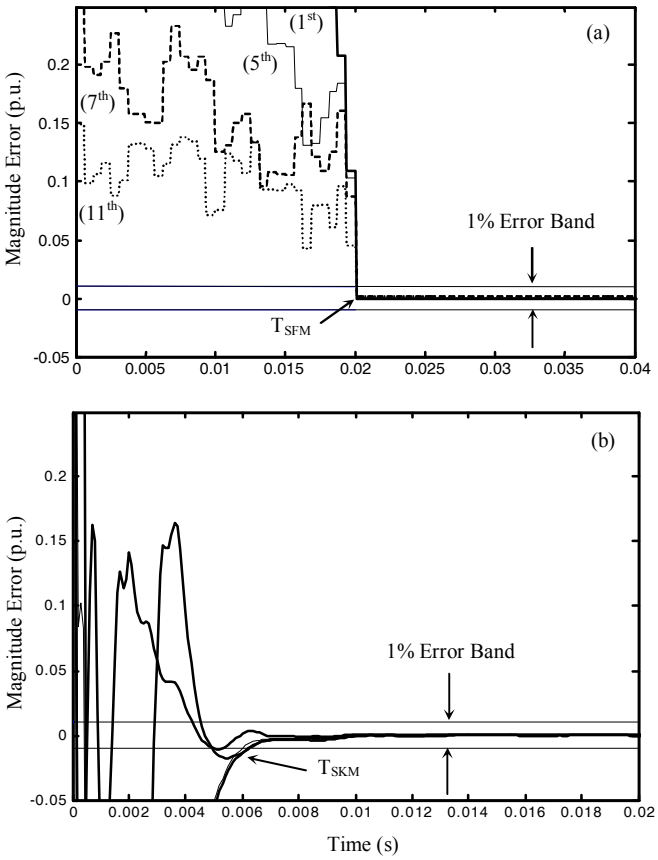

Fig. 4. Harmonics magnitude errors for the (a) OFS FFT, and (b) proposed algorithms.

B. Application

The proposed algorithm is applied in the identification of harmonic content of voltage and current waveforms at point of common coupling between HVAC and HVDC power systems. The system examined in this application was the CIGRE benchmark system (±500 kV, 1000 MW, 12-pulse) [15]. The rectifier converter is operating in constant-current control mode and the inverting converter is operating in a constant-extinction-angle-control mode. The current was sensed at the rectifier-transformer secondary. The voltage and current waveforms obtained under these conditions are shown in Fig. 5. The effect of commutation periods is evident in the waveforms, and the results show that the estimated signals are in good agreement with the original signals.

The acquired voltage and current harmonic properties are shown in Fig. 6 and Fig. 7. These figures show that all the magnitudes of the harmonics are time varying because of the continuous regulation of the firing angle of the HVDC converters to maintain a constant-current output.

V. CONCLUSION

A fast algorithm based on discrete Kalman filtering has been developed and its performance is presented. It is applied to the on-line identification and tracking of the time-varying harmonic content of distorted voltage and current waveforms at the point of common coupling between

HVAC and HVDC power systems. The success of the procedure in accurately estimating dynamic harmonic properties has been illustrated. An accurate estimation has been shown to be possible using the proposed algorithm with a small data window size. The output of the algorithm is compared with output of an OFS FFT algorithm. The results show that the algorithm output converges to a low error significantly faster than the FFT and has a lower steady-state.

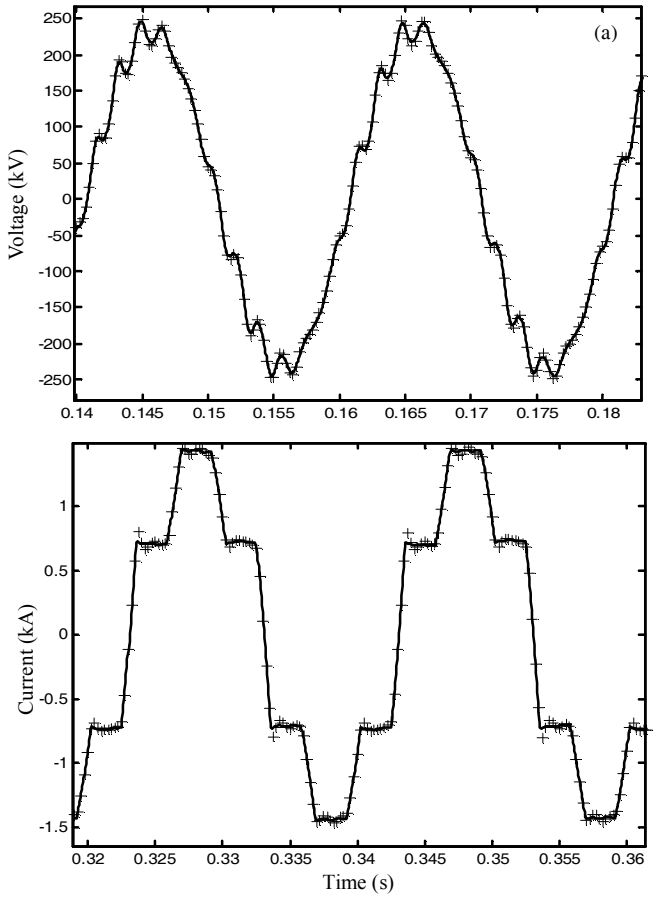

Fig. 5. Voltage and current waveforms (line) and their identification (+) at the point of common coupling between HVAC and HVDC systems.

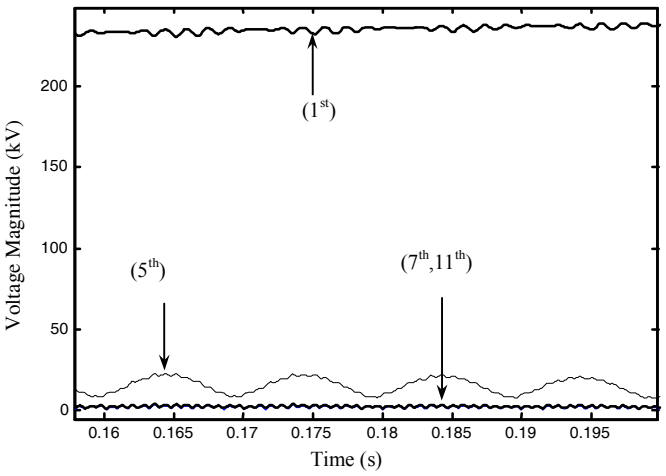

Fig. 6. Voltage harmonic identification at the point of common coupling between HVAC and HVDC systems.

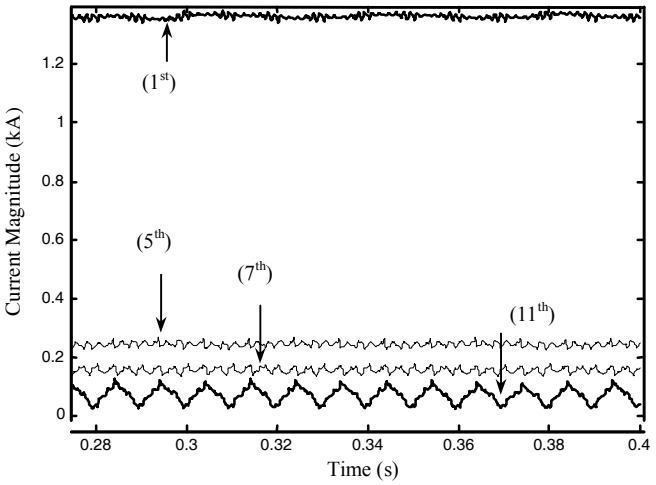

Fig. 7. Current harmonic identification at the point of common coupling between HVAC and HVDC systems.

These benefits are very important for harmonic identification during transient and dynamic operation to allow timely and effective HVDC converter regulation or remedial action.

REFERENCES

[1] J. Arrillaga, B. Smith, AC-DC power system analysis. London: IEE Power and energy series, 1998.

[2] A.A. Girgis, W.B. Chang, E.B. Makram, "A digital recursive measurement scheme for on-line tracking of power system harmonics," IEEE Trans Power Delivery 1991; 6(2): 1153-1160.

[3] J.S. Throp, A.G. Phadke, K.J. Karimi, "Real-time voltage phasor measurements for static-state estimation," IEEE Trans Power Apparatus and Systems 1985; 104(11): 3099-3106.

[4] G.T. Heydt, "A new method for the calculation of sub-transmission and distribution system transients based on the FFT," IEEE Trans Power Delivery 1989; 4(3): 1869-1875.

[5] A.A. Girgis, F.A. Ham, "Qualitative study of pitfalls in FFT," IEEE Trans Aerospace Systems 1980; 16(4): 434-439.

[6] "Time-varying harmonics: part1- characterizing measured data," Aspect Task Force of the Harmonics Working Group, IEEE Trans Power Delivery 1998; 13(3): 938-944.

[7] T.P. Tsao, R.C. Wu, C.C. Nig, "The optimization of spectral analysis for signal harmonics," IEEE Trans Power Delivery2001; 16(2: 149-153.

[8] S.A. Soliman, G.S. Christensen, K.M. El-Nagar, "A state estimation algorithm for identification and measurement of power system harmonics," Electric Power System Research Journal, 1990, Vol.19, 195-206.

[9] S.A. Soliman, A.M. Al-Kandari, K.M. El-Nagar, El-Hawary, "New dynamic filter based on least absolute value algorithm for on-line tracking of power system harmonics," IEE Proc. Generation Transmission Distribution 1995; 142(1):37-44.

[10] E.A. Abu, E.A. Al-Feilat, I. El-Amin, M. Bettayeb, " Power system harmonic estimation: a comparative study," Electric Power System Research Journal, Vol.29, 1994, 91-97.

[11] M.A. Mostafa, "Kalman filtering algorithm for electric power quality analysis: harmonics and voltage sag problems," Proceedings of the Large Engineering Systems Power Quality Conference, May 2003, 110-119.

[12] A.V. Balakrishnan, Kalman filtering theory, New York: Optimization Software Publications Division, 1987.

[13] R.G. Brown. Introduction to random signal analysis and Kalman filtering. New York: John Wiley & Sons, 1983.

[14] PSCAD/EMTDC user's Guide. Manitoba HVDC Research Centre, 1999.

[15] M. Szechtman, T. Wess, C.V. Thio, "First benchmark model for HVDC control studies," Electra, April 1991, No. 135